

Probing Fermi-surface spin-textures via the nonlinear Shubnikov-de Haas effect

Kazuki Nakazawa,¹ Henry F. Legg,^{2,3} Renato M. A. Dantas,³ Jelena Klinovaja,³ and Daniel Loss^{3, 1, 4, 5, 6}

¹RIKEN Center for Quantum Computing (RQC), 2-1 Hirosawa, Wako, Saitama 351-0198, Japan

²SUPA, School of Physics and Astronomy, University of St Andrews,
North Haugh, St Andrews, KY16 9SS, United Kingdom

³Department of Physics, University of Basel, Klingelbergstrasse 82, 4056 Basel, Switzerland

⁴Physics Department, King Fahd University of Petroleum and Minerals, 31261, Dhahran, Saudi Arabia

⁵Quantum Center, KFUPM, Dhahran, Saudi Arabia

⁶RDIA Chair in Quantum Computing

(Dated: January 21, 2026)

The coupling of spin and electronic degrees of freedom via the spin-orbit interaction (SOI) is an essential ingredient for many proposed future technologies. However, probing the strength and nature of SOI is a significant challenge, especially in heterostructures. Here, we consider the nonlinear Shubnikov-de Haas (NSdH) effect, a quantum oscillatory effect that occurs under conditions similar to those of the well-known SdH effect, but is second order in the applied electric field. We demonstrate that, unlike its linear counterpart, the NSdH effect is highly sensitive to the spin textures that arise from SOI. In particular, we show that the phase and beating of NSdH oscillations in nonlinear conductivities can clearly distinguish between different types of SOI. As a demonstration, we show how NSdH can distinguish between the linear and cubic Rashba couplings that are expected in germanium heterostructures. Our results establish the NSdH effect as a powerful and sensitive probe of SOI, offering a new framework for characterizing materials relevant to topology, spintronics, and solid-state quantum information technologies.

Introduction.—The spin-orbit interaction (SOI) is a cornerstone of modern condensed matter physics, driving key fields such as spintronics [1–3], topological matter [4], and quantum information processing [5–11], while also underpinning fundamental phenomena including the anomalous and spin Hall effects [12–20], the Dzyaloshinskii–Moriya interaction [21, 22], and topological electronic band structures [4, 23–25]. The ability to electrically tune SOI in low-dimensional systems [26–37], such as semiconductor nanostructures, is particularly important, enabling benefits such as longer spin-relaxation lengths [38–40]. For instance, the combination of strong SOI with magnetic fields and tailored device geometries can be exploited to suppress noise and improve spin qubit performance [35–37]. The ability to characterize SOI and corresponding Fermi-surface spin textures is therefore of critical importance for future technologies.

A traditional method to detect features of a Fermi surface is the Shubnikov-de Haas (SdH) effect; the formation of Landau levels in a strong magnetic field leads to sharp modulations in the electronic density of states, which in turn result in oscillations of the longitudinal conductivity perpendicular to the magnetic field [41–49]. The period of SdH oscillations is inversely proportional to the magnetic field strength, B , and is directly proportional to the extremal area of the Fermi surface perpendicular to the magnetic field, F_i . This relationship between period and area means that SdH oscillations can map out the Fermi-surface of a solid [45].

Despite the development of other powerful techniques such as angle-resolved photoemission spectroscopy, the SdH effect remains a common method for probing the structure of Fermi surfaces. Generically, for a Fermi sur-

face that is spin-split due to SOI, i.e. containing two portions with areas F_1 and F_2 , the SdH effect will take the form $\sigma_{xx} \sim a_1 \cos(F_1/B) + a_2 \cos(F_2/B)$, where σ_{xx} is the longitudinal conductivity. Typically the amplitudes a_1 and a_2 increase with magnetic field, and the phase of the two SdH contributions from each Fermi-surface is the same. Unfortunately this means that, while the SOI strength can be detected from a beating of the SdH oscillations [26, 46, 50, 51], it is a subtle effect. In particular, observing SOI-related features from the SdH effect often requires large magnetic fields, and signatures are easily smeared out by temperature and disorder.

Recently, nonlinear transport phenomena, i.e. higher-order responses to external driving forces, have been suggested as a new probe of SOI [52–55]. Nonlinear transport has been extensively studied in systems without inversion symmetry and has revealed novel material functionalities [53–73]. This interest has also led to microscopic formulations of nonlinear transport phenomena that highlight the roles of band geometry, spin texture, and the orbital magnetic moment arising from interband contributions [55, 60–62, 67, 71, 74].

In this work, we introduce the nonlinear Shubnikov-de Haas (NSdH) effect, which describes SdH oscillations arising from the second-order response to an electric field. We demonstrate that this effect provides a highly sensitive probe of the SOI-induced spin texture on the Fermi surface. A typical measurement setup is illustrated in Fig. 1(a). First, we formulate the NSdH effect using the Keldysh Green function method and derive a general expression for the second-order conductivity tensor in the Landau-level basis. We then examine the conditions for NSdH oscillations to occur and,

as an example, apply our formalism to two-dimensional hole gases with linear and cubic SOI, as found in germanium (Ge) heterostructures [8, 54, 55, 75, 76]. Generally, we find that the NSdH conductivity takes the form $\sigma_{xii} \sim b_1 \cos(F_1/B) - b_2 \cos(F_2/B)$, where the opposite signs of the coefficients b_1 and b_2 signify a crucial π -phase difference between different Fermi-surface contributions. This phase shift is a direct consequence of the Fermi-surface spin texture, and makes SOI signatures in the NSdH effect considerably more pronounced than in linear SdH. Furthermore, we find that phase differences between components of the full NSdH conductivity tensor are strongly dependent on the symmetry of the underlying SOI term in the Hamiltonian, meaning that a full analysis of the NSdH effect can provide a detailed characterization of the SOI effects in a system.

Formulation.—We start with the derivation of the second-order response current to the electric field in the Landau-level basis. In the Keldysh formalism, the statistical average of the current density is given by

$$j_i \equiv \langle \hat{j}_i \rangle = -\frac{i}{2} \int \frac{d\varepsilon}{2\pi} \text{tr}[\hat{j}_i \hat{G}^K], \quad (1)$$

where \hat{G}^K is the Keldysh Green function, $\hat{j}_i = -\delta \hat{H}/\delta A_i$ is the i^{th} component of the electric current density operator, and tr denotes the trace over all degrees of freedom. To isolate the effect of the electric field, we separate the vector potential into space- and time-dependent parts $\mathbf{A}(\mathbf{r}, t) \equiv \mathbf{A}'(\mathbf{r}) + \mathbf{A}''(t)$ and introduce the total and static kinetic momenta, $\hat{\mathbf{\Pi}} \equiv -i\hbar \nabla + e\mathbf{A}(\mathbf{r}, t)$ and $\hat{\mathbf{\pi}} \equiv -i\hbar \nabla + e\mathbf{A}'(\mathbf{r})$, respectively. Here, e is the elementary charge ($e > 0$). We thus define the static magnetic field $\mathbf{B} = \nabla \times \mathbf{A}'(\mathbf{r})$ and the uniform electric field $\mathbf{E} = -\partial_t \mathbf{A}''(t)$. In order to calculate the higher-order responses to \mathbf{E} , we expand the Hamiltonian \hat{H} and the current operator \hat{j}_i in powers of $\mathbf{A}''(t)$ to expand \hat{G}^K in terms of the coupling term $\hat{H}(\hat{\mathbf{\Pi}}) - \hat{H}(\hat{\mathbf{\pi}}) \equiv \int \frac{d\omega}{2\pi} \hat{X}_i(-\omega) A''_i(\omega)$ (see Supplemental Material (SM) [77]). Hereafter, we focus on the second-order response to the electric field. We first obtain the second-order ac current $j_i^{(2)}(\omega_1, \omega_2)$ at finite injected field frequencies ω_1 and ω_2 , and then take the dc limit, retaining the nondivergent (regular) part [55, 62, 77, 78].

If we assume that the model is described by a function of the static kinetic momentum $\hat{\mathbf{\pi}}$, we can rewrite the Hamiltonian in terms of the ladder operators $\hat{a} = \frac{\ell_B}{\sqrt{2\hbar}}(\hat{\pi}_x - i\hat{\pi}_y)$ and $\hat{a}^\dagger = \frac{\ell_B}{\sqrt{2\hbar}}(\hat{\pi}_x + i\hat{\pi}_y)$, where $\ell_B \equiv \sqrt{\hbar/|eB_z|}$ is the magnetic length. To perform the numerical calculations, we move to the Landau-level basis $|n\rangle$, where n specifies the Landau level ($\varepsilon_n = \langle n|\hat{H}|n\rangle$). Defining $\Gamma_i^{nm} \equiv \langle n|\hat{\Gamma}_i|m\rangle$, $\Gamma_{ij}^{nm} \equiv \langle n|\hat{\Gamma}_{ij}|m\rangle$, and $\Lambda_i^{nm} \equiv \langle n|\hat{\Lambda}_i|m\rangle$, which are the matrix elements of the expansion coefficients of the Hamiltonian and the current operator (see SM [77]), and working at $T = 0$ K, we obtain the second-order conductivity tensor σ_{ijl} in the dc limit, de-

fined by $\langle \hat{j}_i^{(2)} \rangle = \sigma_{ijl} E_j E_l$, whose explicit form is given in Eq. (2) [55, 62, 74, 77].

$$\sigma_{ijl} \simeq -\frac{\hbar^2}{2\pi} N_L \text{Im} \sum_{nml}^{2N} \Lambda_i^{nm} (G_m^R)^2 \times \left(\Gamma_j^{ml} G_\ell^R \Gamma_l^{ln} + \Gamma_l^{ml} G_\ell^R \Gamma_j^{ln} + \frac{\Gamma_{jl}^{mn}}{N} \right) (G_n^R - G_n^A), \quad (2)$$

where $G_n^R \equiv [\mu - \varepsilon_n - \Sigma^R(\mu)]^{-1} = (G_n^A)^\dagger$, with the retarded self-energy $\Sigma^R(\mu)$ at the chemical potential μ , N_L is the Landau degeneracy per unit area, N is the number of the Landau levels considered in the computation, and n, m, ℓ are the Landau level indices. N_L appears after integrating over the in-plane degrees of freedom in the presence of the Landau quantization [47, 79, 80]. This expression is similar to results obtained in previous studies, where the conductivity was presented in the momentum representation [62, 74]. However, note that here the Green functions contain all the information about the out-of-plane component of the magnetic field and the Landau-level structure, describing the orbital motion of an electron. See SM for further details of the derivation [77].

For comparison, we also calculate the linear longitudinal conductivity using the Kubo formula [47, 78],

$$\sigma_{ij} = \frac{\hbar N_L}{2\pi} \sum_{nm} \Gamma_i^{nm} G_m^R \Gamma_j^{mn} G_n^A. \quad (3)$$

Here, we neglect $G^R G^R$ and $G^A G^A$ terms since they are subdominant in the longitudinal component ($i = j$) [47].

The self-energy is evaluated within the self-consistent Born approximation (SCBA), including an imaginary constant component $i\gamma_c$ which captures the level broadening arising from various sources (e.g., scattering by phonons),

$$\Sigma^R(\mu) = i n_i u^2 N_L \sum_n \text{Im} G_n^R(\mu) - i\gamma_c. \quad (4)$$

Here, n_i and u are the impurity concentration and the strength of the impurity scattering, respectively. Henceforth, we take $\gamma_c = 0.01$ meV. Otherwise, we employ an imaginary constant self-energy $\Sigma^R = -i\gamma$ since the self-consistent treatment does not make an essential difference in our case [77]. We employed SCBA in Fig. 1 and imaginary constant self-energy in Fig. 2.

NSdH effect as a probe of spin textures.—We now relate the nonlinear conductivity derived above to the spin texture in the generic model $H_{\mathbf{k}} = h_{\mathbf{k}} + \bar{\mathbf{S}}_{\mathbf{k}} \cdot \boldsymbol{\sigma}$ where $h_{\mathbf{k}}$ and $\bar{\mathbf{S}}_{\mathbf{k}}$ are assumed to be even and odd functions of the wave vector \mathbf{k} , respectively. The nonlinear conductivity σ_{xii} for an in-plane field can be calculated perturbatively in the spin texture term, $\bar{\mathbf{S}}_{\mathbf{k}} \cdot \boldsymbol{\sigma}$, yielding

$$\sigma_{ijl} = \frac{6e^3}{\pi\hbar} \sum_{\mathbf{k}} \mathcal{K}_{\mathbf{k}} \bar{\mathbf{S}}_{\mathbf{k}} \cdot [\mathcal{V}_{(j} \partial_l \partial_{i)} + \mathcal{V}_{(j l} \partial_{i)}] \bar{\mathbf{S}}_{\mathbf{k}}, \quad (5)$$

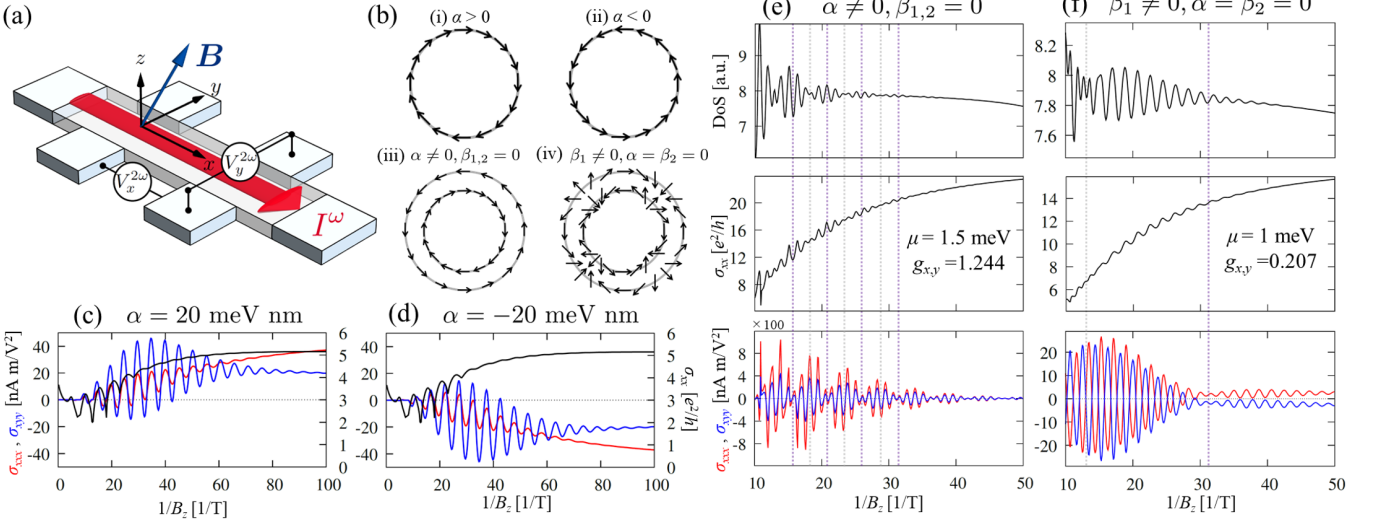


FIG. 1. **Phenomenology of NSdH effect.** (a) Schematic of our setup. We assume a lock-in measurement in which a low-frequency ac current I^ω (corresponding to an ac electric field $E(\omega)$ in our theoretical framework) is injected, and the 2ω components of the longitudinal and Hall voltages are read out. (b) Schematic illustrations of the in-plane spin textures on the Fermi surface at $B = 0$. They correspond to (i,ii) single-Fermi-surface cases of $\mathbf{S}_k^{(1)}$ with (i) $\alpha > 0$, $\beta_2 = 0$ and (ii) $\alpha < 0$, $\beta_2 = 0$, and (iii,iv) two-Fermi-surface cases for (iii) $\mathbf{S}_k^{(1)}$ and (iv) $\mathbf{S}_k^{(3)}$, respectively. (c,d) Linear (black lines) and nonlinear SdH oscillations (red: σ_{xxx} , blue: σ_{xyy}) for the model exhibiting a single Fermi surface with (c) $\alpha = 20$ meV nm and (d) $\alpha = -20$ meV nm. We set $m^* = \infty$, $\lambda = 20$ nm, $\beta_{1,2} = 0$ meV nm 3 , $g_{x,y} = 1.244$, $g_z = 10$, $(B_x, B_y) = (0$ T, 0.1 T), and $\mu = 0.6$ meV in both cases. We set the impurity-scattering parameter to $n_i u^2 = 100$ meV 2 nm 2 . (e,f) Density of states (DoS), and linear and nonlinear SdH oscillations for 2DHGs. We consider $\hbar^2/(2m^*) = 620$ meV nm 2 , $\lambda = 0$, and $g_z = 10$ with (e) $\alpha = 1.5$ meV nm, $\beta_{1,2} = 0$, $g_{x,y} = 1.244$, and (f) $\beta_1 = 190$ meV nm 3 , $\alpha = \beta_2 = 0$, $g_{x,y} = 0.207$, inspired by the Ge [110] and Ge [100] cases, respectively [8, 54, 55, 76]. We employ an in-plane magnetic field of $(B_x, B_y) = (0$ T, 5 T), and set the impurity parameter to $n_i u^2 = 60$ meV 2 nm 2 . Purple and gray dotted lines indicate the positions of the beating nodes in σ_{xii} and σ_{xx} , respectively. We use a sufficiently large number of Landau levels, $N = 400$, in all panels (c)–(f).

where $\partial_i \equiv \partial/\partial k_i$, $\mathcal{V}_i = \partial_i h_{\mathbf{k}}$, $\mathcal{V}_{ij} = \partial_i \partial_j h_{\mathbf{k}}$, and $\mathcal{K}_{\mathbf{k}}$ is the imaginary part of a product of Green functions [77]. The parentheses around the indices indicates total symmetrization. It is important to note that Eq. (5) demonstrates how the geometry of the Fermi-surface spin texture is directly linked to the nonlinear conductivity. In particular, the first term in the square brackets depends on the curvature of the spin texture and the second term on the derivative of the spin texture.

As a concrete example, we consider the NSdH in an effective model of a two-dimensional electron (hole) gas [2DE(H)G] with linear and cubic Rashba SOI; the cubic term containing both isotropic and anisotropic interactions. The system is subject to a magnetic field with out-of-plane and in-plane components, such that the out-of-plane field produces orbital effects, while the in-plane field generates a Zeeman coupling [54, 55]. The corresponding Hamiltonian is

$$\hat{H} = \frac{\hat{\Pi}^2}{2m^*} + \tilde{\alpha}(\boldsymbol{\sigma} \times \hat{\Pi}) \cdot \hat{z} + i\tilde{\beta}_1(\hat{\Pi}_+^3 \sigma_- - \hat{\Pi}_-^3 \sigma_+) + i\tilde{\beta}_2(\hat{\Pi}_+ \hat{\Pi}_- \hat{\Pi}_+ \sigma_+ - \hat{\Pi}_- \hat{\Pi}_+ \hat{\Pi}_- \sigma_-) + \Delta \cdot \boldsymbol{\sigma}, \quad (6)$$

where m^* is an effective mass, $\tilde{\alpha} \equiv (\alpha/\hbar)(1 + \lambda^2 \hat{\Pi}^2/\hbar^2)$ [81], and $\tilde{\beta}_{1,2} \equiv \beta_{1,2}/\hbar^3$ specify the strengths

of the linear and cubic Rashba SOI, respectively; $\hat{\Pi}_{\pm} \equiv \hat{\Pi}_x \pm i\hat{\Pi}_y$, $\boldsymbol{\sigma} = (\sigma_x, \sigma_y, \sigma_z)$ is the vector of Pauli matrices, $\sigma_{\pm} = (\sigma_x \pm i\sigma_y)/2$, and $\Delta = (\mu_B/2)(g_x B_x, g_y B_y, g_z B_z)$ with μ_B and g_i denoting the Bohr magneton and effective g -factors, respectively. Note that, in this model, a finite in-plane component of the magnetic field is essential to observe a finite nonlinear conductivity. The parameter λ allows us to modify the band structure to realize only a single Fermi-surface with spin-momentum locking, as found, e.g., on the surface of a topological insulator [81]. The corresponding wave vector representation is obtained by setting $h_{\mathbf{k}} = (\hbar \mathbf{k})^2/(2m^*)$ and $\bar{\mathbf{S}}_{\mathbf{k}} = \mathbf{S}_{\mathbf{k}} + \Delta$, where $\mathbf{S}_{\mathbf{k}} = \mathbf{S}_{\mathbf{k}}^{(1)} + \mathbf{S}_{\mathbf{k}}^{(3)}$ with

$$\mathbf{S}_{\mathbf{k}}^{(1)} = [\alpha k(1 + \lambda^2 k^2) - \beta_2 k^3](\sin \phi_{\mathbf{k}}, \cos \phi_{\mathbf{k}}, 0), \quad (7)$$

$$\mathbf{S}_{\mathbf{k}}^{(3)} = \beta_1 k^3(\sin 3\phi_{\mathbf{k}}, \cos 3\phi_{\mathbf{k}}, 0), \quad (8)$$

and $\tan \phi_{\mathbf{k}} = k_y/k_x$ [75, 82–85]. $\mathbf{S}_{\mathbf{k}}^{(1)}$ and $\mathbf{S}_{\mathbf{k}}^{(3)}$ specify the in-plane spin texture on a given isoenergy contour. As seen in Eq. (5), the curvature of the spin texture is relevant in the presence of the cubic terms. The nonlinear conductivity changes sign when the spin texture is inverted (i.e. $\mathbf{S}_{\mathbf{k}} \rightarrow -\mathbf{S}_{\mathbf{k}}$), as in previous studies [52–55].

First, we discuss the SdH and NSdH oscillations calculated using Eqs. (2) and (3) for a single Fermi-surface

with spin-momentum locking ($\beta_1 = \beta_2 = 0$) [81]. Figs. 1(c) and (d) show the B_z dependence of the linear longitudinal conductivity σ_{xx} and the second-order nonlinear conductivity σ_{xii} for two cases characterized by opposite signs of the linear Rashba parameter. Depending on the sign of α , the spin textures characterized by $S_{\mathbf{k}}^{(1)}$ have opposite directions [see Figs. 1(b) (i) and (ii)], and correspondingly, the sign of the nonlinear conductivity σ_{xii} is also opposite, which appears as an inversion of the oscillation phase. In contrast, linear SdH oscillations in σ_{xx} are insensitive to the sign of α , i.e., the spin-texture on the Fermi-surface.

Next, we consider a more realistic effective model of a Ge-based planar heterostructure by adopting the appropriate parameters [8, 54, 55, 76]. Figures 1(e) and (f) show the contrast between quantum oscillations for two simplified SOI models: (a) a purely linear α term, and (b) a purely cubic β_1 term. These models approximate Ge [110] and Ge [100] surfaces at low chemical potentials and feature distinct spin textures with one and three rotations per isoenergy contour, respectively [see Figs. 1(b) (iii) and (iv)]. In both models, when $B = 0$, the spin textures of the inner and outer Fermi-surfaces are oppositely oriented, as required by time-reversal symmetry.

This example demonstrates the key features that make NSdH effect a highly sensitive probe of spin-textures. First, while both the linear SdH (σ_{xx}) and nonlinear NSdH (σ_{xii}) effects exhibit beating, their node positions alternate, which underscores how the two effects are influenced by spin-split bands. Linear SdH oscillations are sensitive to the total density of states, and the beatings arises when there is constructive interference of signals from both Fermi surfaces. In contrast, as discussed above, the NSdH effect is directly sensitive to the spin texture. Since the textures on the inner and outer surfaces are opposite to each other, their contributions to the nonlinear conductivity exhibit a π -phase shift between them. This phase difference is pivotal: while linear SdH merges both bands into a single beating envelope, the NSdH signal flips sign depending on the dominant Fermi surface contribution, directly exposing the competing NSdH contributions arising from the SOI-induced spin-texture.

Furthermore, NSdH is not only sensitive to the presence and direction of a Fermi surface spin texture, but also provides a tool to distinguish SOIs with different symmetries. In particular, using the different components of the conductivity tensor, we can distinguish the linear and cubic Rashba SOI found in our Ge 2DHG example. For purely linear SOI (α) the longitudinal σ_{xxx} and Hall σ_{xyy} nonlinear conductivities are in-phase, while for purely cubic SOI (β_1), they are perfectly out-of-phase [Figs. 1(e) and (f)]. This is a direct consequence of the underlying symmetry of the SOI term in each case. In fact, for cubic SOI in our model, symmetry enforces the

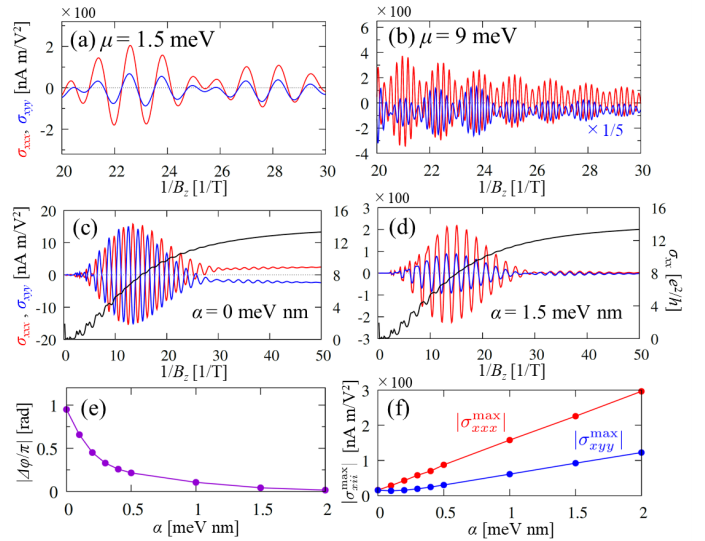


FIG. 2. Spin texture dependence of NSdH effect. (a,b) Chemical-potential dependence of the nonlinear SdH oscillations for Ge [110] parameters (i.e. $\alpha = 1.5$ meV nm, $\beta_1 = 190$ meV nm 3 , $\beta_2 = 23.75$ meV nm 3 , and $g_{x,y} = 1.244$). We set (a) $\mu = 1.5$ meV and (b) $\mu = 9$ meV. The plot of σ_{xyy} in (b) is magnified by a factor of five to make the phase difference relative to σ_{xxx} visible. (c,d) Linear Rashba SOI dependence of the linear and nonlinear SdH oscillations for Ge [100] parameters (i.e. $\alpha = 0$ meV nm, $\beta_1 = 190$ meV nm 3 , $\beta_2 = 23.75$ meV nm 3 , and $g_{x,y} = 0.207$) at a common chemical potential $\mu = 1$ meV, with (c) $\alpha = 0$ and (d) $\alpha = 1.5$ meV nm. (e,f) α dependence of (e) the phase difference $\Delta\varphi$ between σ_{xxx} and σ_{xyy} and (f) the maximum value of $|\sigma_{xii}|$ for the Ge [100] parameters. For all panels in this figure, we assume a purely imaginary constant self-energy $\gamma = 0.07$ meV [48], and the other parameters are the same as those in Figs. 1(e,f).

exact relation (see SM [77]):

$$\sigma_{xxx} = -\sigma_{xyy}. \quad (9)$$

This relation provides a powerful method to determine the magnitude of cubic SOI using the “antisymmetric component”, $\sigma_{xxx} - \sigma_{xyy}$, of the conductivity tensor and evinces the utility of NSdH to characterize SOI.

Our calculations for realistic Ge heterostructures also demonstrate the experimental feasibility of this approach to characterizing SOI. By tuning the chemical potential or the linear Rashba strength (α)—both experimentally controllable via gate voltages—we can directly track the evolution of this symmetric component and corresponding ratios of cubic to linear SOI (Fig. 2). Finally, we note that the features shown in the nonlinear conductivity—as calculated in theory—should be observable even in the nonlinear resistivity—as measured in experiments (see SM [77] for details).

Discussion.—We have established the nonlinear Shubnikov–de Haas (NSdH) effect as a highly sensitive probe of SOI. Unlike conventional linear SdH oscillations,

which are only weakly sensitive to the underlying spin-texture and spin-split Fermi surface, the NSdH effect can distinguish between different forms of SOI, such as linear and cubic Rashba couplings. The distinctive interference patterns and symmetries imprinted on the nonlinear conductivity oscillations provide a direct method for characterizing the spin textures of materials, thereby offering a crucial tool for parameterizing devices for spintronics and quantum information technologies applications.

K.N. thanks H. Isobe, A. Yamada, and T. Yamaguchi for the helpful discussions. K.N. is supported by JSPS KAKENHI Grant Number JP21K13875. This work was supported as a part of NCCR SPIN, a National Centre of Competence in Research, funded by the Swiss National Science Foundation (grant number 225153). D.L. acknowledges the Deanship of Research and the Quantum Center for the support received under Grant no. CUP25102 and no. INQC2500, respectively.

[1] I. Žutić, J. Fabian, and S. Das Sarma, Spintronics: Fundamentals and applications, *Rev. Mod. Phys.* **76**, 323 (2004).

[2] S. D. Bader and S. S. P. Parkin, Spintronics, *Annual Review of Condensed Matter Physics* **1**, 71 (2010).

[3] A. Hirohata, K. Yamada, Y. Nakatani, I.-L. Prejbeanu, B. Diény, P. Pirro, and B. Hillebrands, Review on spintronics: Principles and device applications, *J. Magn. Magn. Mater.* **509**, 166711 (2020).

[4] N. P. Armitage, E. J. Mele, and A. Vishwanath, Weyl and Dirac semimetals in three-dimensional solids, *Rev. Mod. Phys.* **90**, 015001 (2018).

[5] D. Loss and D. P. DiVincenzo, Quantum computation with quantum dots, *Phys. Rev. A* **57**, 120 (1998).

[6] R. Hanson, L. P. Kouwenhoven, J. R. Petta, S. Tarucha, and L. M. K. Vandersypen, Spins in few-electron quantum dots, *Rev. Mod. Phys.* **79**, 1217 (2007).

[7] C. Kloeffel and D. Loss, Prospects for Spin-Based Quantum Computing in Quantum Dots, *Annu. Rev. Condens. Matter Phys.* **4**, 51 (2013).

[8] G. Scappucci, C. Kloeffel, F. A. Zwanenburg, D. Loss, M. Myronov, J.-J. Zhang, S. De Franceschi, G. Katsaros, and M. Veldhorst, The germanium quantum information route, *Nat. Rev. Mater.* **6**, 926 (2021).

[9] N. W. Hendrickx, W. I. L. Lawrie, L. Petit, A. Sammak, G. Scappucci, and M. Veldhorst, A single-hole spin qubit, *Nat. Commun.* **11**, 3478 (2020).

[10] N. W. Hendrickx, D. P. Franke, A. Sammak, G. Scappucci, and M. Veldhorst, Fast two-qubit logic with holes in germanium, *Nature* **577**, 487 (2020).

[11] N. W. Hendrickx, W. I. L. Lawrie, M. Russ, F. van Rijgelen, S. L. de Snoo, R. N. Schouten, A. Sammak, G. Scappucci, and M. Veldhorst, A four-qubit germanium quantum processor, *Nature* **591**, 580 (2021).

[12] R. Karplus and J. M. Luttinger, Hall Effect in Ferromagnetics, *Phys. Rev.* **95**, 1154 (1954).

[13] N. Nagaosa, J. Sinova, S. Onoda, A. H. MacDonald, and N. P. Ong, Anomalous Hall effect, *Rev. Mod. Phys.* **82**, 1539 (2010).

[14] M. I. Dyakonov and V. I. Perel, Current-induced spin orientation of electrons in semiconductors, *Phys. Lett. A* **35**, 459 (1971).

[15] M. I. Dyakonov and V. I. Perel, Possibility of Orienting Electron Spins with Current, *Sov. Phys. JETP* **13**, 467 (1971).

[16] S. Murakami, N. Nagaosa, and S.-C. Zhang, Dissipationless Quantum Spin Current at Room Temperature, *Science* **301**, 1348 (2003).

[17] J. Sinova, D. Culcer, Q. Niu, N. A. Sinitsyn, T. Jungwirth, and A. H. MacDonald, Universal Intrinsic Spin Hall Effect, *Phys. Rev. Lett.* **92**, 126603 (2004).

[18] O. Chalaev and D. Loss, Spin-Hall conductivity due to Rashba spin-orbit interaction in disordered systems, *Phys. Rev. B* **71**, 245318 (2005).

[19] O. Chalaev and D. Loss, Spin-orbit-induced anisotropic conductivity of a disordered two-dimensional electron gas, *Phys. Rev. B* **80**, 035305 (2009).

[20] M. Duckheim, D. L. Maslov, and D. Loss, Dynamic spin-Hall effect and driven spin helix for linear spin-orbit interactions, *Phys. Rev. B* **80**, 235327 (2009).

[21] I. Dzyaloshinsky, A thermodynamic theory of “weak” ferromagnetism of antiferromagnetics, *Journal of Physics and Chemistry of Solids* **4**, 241 (1958).

[22] T. Moriya, Anisotropic Superexchange Interaction and Weak Ferromagnetism, *Phys. Rev.* **120**, 91 (1960).

[23] C. L. Kane and E. J. Mele, Z_2 Topological Order and the Quantum Spin Hall Effect, *Phys. Rev. Lett.* **95**, 146802 (2005).

[24] L. Fu and C. L. Kane, Topological insulators with inversion symmetry, *Phys. Rev. B* **76**, 045302 (2007).

[25] M. Z. Hasan and C. L. Kane, Colloquium: Topological insulators, *Rev. Mod. Phys.* **82**, 3045 (2010).

[26] J. Nitta, T. Akazaki, H. Takayanagi, and T. Enoki, Gate Control of Spin-Orbit Interaction in an Inverted $\text{In}_{0.53}\text{Ga}_{0.47}\text{As}/\text{In}_{0.52}\text{Al}_{0.48}\text{As}$ Heterostructure, *Phys. Rev. Lett.* **78**, 1335 (1997).

[27] C. Kloeffel, M. Trif, and D. Loss, Strong spin-orbit interaction and helical hole states in Ge/Si nanowires, *Phys. Rev. B* **84**, 195314 (2011).

[28] C. Kloeffel, M. J. Rančić, and D. Loss, Direct Rashba spin-orbit interaction in Si and Ge nanowires with different growth directions, *Phys. Rev. B* **97**, 235422 (2018).

[29] C. Adelsberger, M. Benito, S. Bosco, J. Klinovaja, and D. Loss, Hole-spin qubits in Ge nanowire quantum dots: Interplay of orbital magnetic field, strain, and growth direction, *Phys. Rev. B* **105**, 075308 (2022).

[30] C. Adelsberger, S. Bosco, J. Klinovaja, and D. Loss, Enhanced orbital magnetic field effects in Ge hole nanowires, *Phys. Rev. B* **106**, 235408 (2022).

[31] F. Gao, J.-H. Wang, H. Watzinger, H. Hu, M. J. Rančić, J.-Y. Zhang, T. Wang, Y. Yao, G.-L. Wang, J. Kukulčka, L. Vukušić, C. Kloeffel, D. Loss, F. Liu, G. Katsaros, and J.-J. Zhang, Site-Controlled Uniform Ge/Si Hut Wires with Electrically Tunable Spin-Orbit Coupling, *Advanced Materials* **32**, 1906523 (2020).

[32] B. Venitucci, L. Bourdet, D. Pouzada, and Y.-M. Niquet, Electrical manipulation of semiconductor spin qubits within the g -matrix formalism, *Phys. Rev. B* **98**, 155319 (2018).

[33] V. P. Michal, B. Venitucci, and Y.-M. Niquet, Longitudinal and transverse electric field manipulation of hole spin-orbit qubits in one-dimensional channels, *Phys. Rev. B* **103**, 045305 (2021).

[34] L. Bellentani, M. Bina, S. Bonen, A. Secchi, A. Bertoni, S. P. Voinigescu, A. Padovani, L. Larcher, and F. Troiani, Toward Hole-Spin Qubits in Si *p*-MOSFETs within a Planar CMOS Foundry Technology, *Phys. Rev. Appl.* **16**, 054034 (2021).

[35] N. Piot, B. Brun, V. Schmitt, S. Zihlmann, V. P. Michal, A. Apra, J. C. Abadillo-Uriel, X. Jehl, B. Bertrand, H. Niebojewski, L. Hutin, M. Vinet, M. Urdampilleta, T. Meunier, Y.-M. Niquet, R. Maurand, and S. D. Franceschi, A single hole spin with enhanced coherence in natural silicon, *Nat. Nanotechnol.* **17**, 1072 (2022).

[36] S. Bosco, B. Hetényi, and D. Loss, Hole Spin Qubits in Si FinFETs With Fully Tunable Spin-Orbit Coupling and Sweet Spots for Charge Noise, *PRX Quantum* **2**, 010348 (2021).

[37] S. Bosco and D. Loss, Hole Spin Qubits in Thin Curved Quantum Wells, *Phys. Rev. Appl.* **18**, 044038 (2022).

[38] A. G. Mal'shukov and K. A. Chao, Waveguide diffusion modes and slowdown of D'yakonov-Perel' spin relaxation in narrow two-dimensional semiconductor channels, *Phys. Rev. B* **61**, R2413 (2000).

[39] A. Sasaki, S. Nonaka, Y. Kunihashi, M. Kohda, T. Bauernfeind, T. Dollinger, K. Richter, and J. Nitta, Direct determination of spin-orbit interaction coefficients and realization of the persistent spin helix symmetry, *Nature Nanotechnology* **9**, 703 (2014).

[40] Y. Kunihashi, H. Sanada, H. Gotoh, K. Onomitsu, M. Kohda, J. Nitta, and T. Sogawa, Drift transport of helical spin coherence with tailored spin-orbit interactions, *Nature Communications* **7**, 10722 (2016).

[41] L. Schubnikov and W. J. de Haas, New phenomena in the resistance change of bismuth crystals in the magnetic field at the temperature of liquid hydrogen (I), *Proc. Royal Netherlands Acad. Arts Sci., Amsterdam* **33**, 363 (1930).

[42] L. Schubnikov and W. J. de Haas, New phenomena in the resistance change of bismuth crystals in the magnetic field at the temperature of liquid hydrogen (II), *Proc. Royal Netherlands Acad. Arts Sci., Amsterdam* **33**, 418 (1930).

[43] I. M. Lifshits and A. M. Kosevich, Theory of Magnetic Susceptibility in Metals at Low Temperature, *Sov. Phys. JETP* **2**, 636 (1956).

[44] I. M. Lifshits and A. M. Kosevich, On the Theory of the Shubnikov-De Haas Effect, *Sov. Phys. JETP* **6**, 67 (1958).

[45] D. Shoenberg, *Magnetic Oscillations in Metals*, Cambridge Monographs on Physics (Cambridge University Press, 1984).

[46] D. R. Candido, S. I. Erlingsson, H. Gramizadeh, J. V. I. Costa, P. J. Weigle, D. M. Zumbühl, and J. C. Egues, Beating-free quantum oscillations in two-dimensional electron gases with strong spin-orbit and Zeeman interactions, *Phys. Rev. Res.* **5**, 043297 (2023).

[47] A. Yamada and Y. Fuseya, Quantum-classical correspondence and dissipative to dissipationless crossover in magnetotransport phenomena, *J. Phys.: Condens. Matter* **36**, 245702 (2024).

[48] J.-Y. Zhang, M. Ming, J.-H. Wang, D.-M. Huang, H. Gao, Y.-X. Chu, B.-X. Fu, H. Q. Xu, and J.-J. Zhang, High-quality Ge/SiGe heterostructure with atomically sharp interface grown by molecular beam epitaxy, *Appl. Phys. Lett.* **125**, 122106 (2024).

[49] D. Costa, L. E. A. Stehouwer, D. D. Esposti, and G. Scappucci, Quantum oscillations in two-dimensional hole gases with competing cyclotron and zeeman energy (2025), arXiv:2509.15268 [cond-mat.mes-hall].

[50] F. Dettwiler, J. Fu, S. Mack, P. J. Weigle, J. C. Egues, D. D. Awschalom, and D. M. Zumbühl, Stretchable Persistent Spin Helices in GaAs Quantum Wells, *Phys. Rev. X* **7**, 031010 (2017).

[51] A. J. A. Beukman, F. K. de Vries, J. van Veen, R. Skolasinski, M. Wimmer, F. Qu, D. T. de Vries, B.-M. Nguyen, W. Yi, A. A. Kiselev, M. Sokolich, M. J. Manfra, F. Nichele, C. M. Marcus, and L. P. Kouwenhoven, Spin-orbit interaction in a dual gated InAs/GaSb quantum well, *Phys. Rev. B* **96**, 241401 (2017).

[52] T. Ideue, K. Hamamoto, S. Koshikawa, M. Ezawa, S. Shimizu, Y. Kaneko, Y. Tokura, N. Nagaosa, and Y. Iwasa, Bulk rectification effect in a polar semiconductor, *Nat. Phys.* **13**, 578 (2017).

[53] Y. Li, Y. Li, P. Li, B. Fang, X. Yang, Y. Wen, D.-X. Zheng, C.-H. Zhang, X. He, A. Manchon, Z.-H. Cheng, and X.-X. Zhang, Nonreciprocal charge transport up to room temperature in bulk Rashba semiconductor α -GeTe, *Nat. Commun.* **12**, 540 (2021).

[54] R. M. A. Dantas, H. F. Legg, S. Bosco, D. Loss, and J. Klinovaja, Determination of spin-orbit interaction in semiconductor nanostructures via nonlinear transport, *Phys. Rev. B* **107**, L241202 (2023).

[55] K. Nakazawa, H. F. Legg, J. Klinovaja, and D. Loss, Interband contributions to nonlinear transport in semiconductor nanostructures, *Phys. Rev. B* **111**, 125305 (2025).

[56] J. E. Sipe and A. I. Shkrebtii, Second-order optical response in semiconductors, *Phys. Rev. B* **61**, 5337 (2000).

[57] Y. Gao, S. A. Yang, and Q. Niu, Field Induced Positional Shift of Bloch Electrons and Its Dynamical Implications, *Phys. Rev. Lett.* **112**, 166601 (2014).

[58] I. Sodemann and L. Fu, Quantum Nonlinear Hall Effect Induced by Berry Curvature Dipole in Time-Reversal Invariant Materials, *Phys. Rev. Lett.* **115**, 216806 (2015).

[59] R. Takashima, Y. Shiomi, and Y. Motome, Nonreciprocal spin Seebeck effect in antiferromagnets, *Phys. Rev. B* **98**, 020401(R) (2018).

[60] D. E. Parker, T. Morimoto, J. Orenstein, and J. E. Moore, Diagrammatic approach to nonlinear optical response with application to Weyl semimetals, *Phys. Rev. B* **99**, 045121 (2019).

[61] S. M. João and J. M. V. P. Lopes, Basis-independent spectral methods for non-linear optical response in arbitrary tight-binding models, *J. Phys.: Condens. Matter* **32**, 125901 (2019).

[62] Y. Michishita and R. Peters, Effects of renormalization and non-hermiticity on nonlinear responses in strongly correlated electron systems, *Phys. Rev. B* **103**, 195133 (2021).

[63] Z. Z. Du, H.-Z. Lu, and X. C. Xie, Nonlinear Hall effects, *Nat. Rev. Phys.* **3**, 744 (2021).

[64] R. M. A. Dantas, Z. Wang, P. Surówka, and T. Oka, Nonperturbative topological current in Weyl and Dirac semimetals in laser fields, *Phys. Rev. B* **103**, L201105 (2021).

[65] K. Nakazawa, Y. Kato, and Y. Motome, Asymmetric modulation of Majorana excitation spectra and nonreciprocal thermal transport in the Kitaev spin liquid under a staggered magnetic field, *Phys. Rev. B* **105**, 165152 (2022).

[66] H. F. Legg, M. Rößler, F. Münnig, D. Fan, O. Bre

unig, A. Bliesener, G. Lippertz, A. Uday, A. A. Taskin, D. Loss, J. Klinovaja, and Y. Ando, Giant magnetochiral anisotropy from quantum-confined surface states of topological insulator nanowires, *Nat. Nanotechnol.* **17**, 696 (2022).

[67] R. Oiwa and H. Kusunose, Systematic analysis method for nonlinear response tensors, *Journal of the Physical Society of Japan* **91**, 014701 (2022).

[68] S. Gholizadeh, J. H. Cullen, and D. Culcer, Nonlinear Hall effect of magnetized two-dimensional spin- $\frac{3}{2}$ heavy holes, *Phys. Rev. B* **107**, L041301 (2023).

[69] R. B. Atencia, D. Xiao, and D. Culcer, Disorder in the nonlinear anomalous hall effect of \mathcal{PT} -symmetric dirac fermions, *Phys. Rev. B* **108**, L201115 (2023).

[70] K. Das, S. Lahiri, R. B. Atencia, D. Culcer, and A. Agarwal, Intrinsic nonlinear conductivities induced by the quantum metric, *Phys. Rev. B* **108**, L201405 (2023).

[71] T. Yamaguchi, K. Nakazawa, and A. Yamakage, Microscopic theory of nonlinear Hall effect induced by electric field and temperature gradient, *Phys. Rev. B* **109**, 205117 (2024).

[72] K. Nakazawa, T. Yamaguchi, and A. Yamakage, Nonlinear charge transport properties in chiral tellurium, *Phys. Rev. Mater.* **8**, L091601 (2024).

[73] K. Nakazawa, T. Yamaguchi, and A. Yamakage, Nonlinear charge and thermal transport properties induced by orbital magnetic moment in chiral crystalline cobalt monosilicide, *Phys. Rev. B* **111**, 045161 (2025).

[74] Y. Michishita and N. Nagaosa, Dissipation and geometry in nonlinear quantum transports of multiband electronic systems, *Phys. Rev. B* **106**, 125114 (2022).

[75] R. Moriya, K. Sawano, Y. Hoshi, S. Masubuchi, Y. Shiraki, A. Wild, C. Neumann, G. Abstreiter, D. Bougeard, T. Koga, and T. Machida, Cubic Rashba Spin-Orbit Interaction of a Two-Dimensional Hole Gas in a Strained-Ge/SiGe Quantum Well, *Phys. Rev. Lett.* **113**, 086601 (2014).

[76] J.-X. Xiong, S. Guan, J.-W. Luo, and S.-S. Li, Emergence of strong tunable linear Rashba spin-orbit coupling in two-dimensional hole gases in semiconductor quantum wells, *Phys. Rev. B* **103**, 085309 (2021).

[77] See Supplemetal Materials at [url] for the calculational details.

[78] R. Kubo, Statistical-Mechanical Theory of Irreversible Processes. I. General Theory and Simple Applications to Magnetic and Conduction Problems, *J. Phys. Soc. Jpn.* **12**, 570 (1957).

[79] J. Schliemann, J. C. Egues, and D. Loss, Variational study of the $\nu = 1$ quantum Hall ferromagnet in the presence of spin-orbit interaction, *Phys. Rev. B* **67**, 085302 (2003).

[80] Y. Fuseya, M. Ogata, and H. Fukuyama, Transport Properties and Diamagnetism of Dirac Electrons in Bismuth, *J. Phys. Soc. Jpn.* **84**, 012001 (2015).

[81] L. Fu, Hexagonal Warping Effects in the Surface States of the Topological Insulator Bi_2Te_3 , *Phys. Rev. Lett.* **103**, 266801 (2009).

[82] L. G. Gerchikov and A. V. Subashiev, Spin splitting of size-quantization subbands in asymmetric heterostructures, *Sov. Phys. Semicond.* **26**, 73 (1992).

[83] J. Schliemann and D. Loss, Spin-Hall transport of heavy holes in III-V semiconductor quantum wells, *Phys. Rev. B* **71**, 085308 (2005).

[84] D. Stepanenko, M. Lee, G. Burkard, and D. Loss, Interference of heavy holes in an Aharonov-Bohm ring, *Phys. Rev. B* **79**, 235301 (2009).

[85] H. Nakamura, T. Koga, and T. Kimura, Experimental Evidence of Cubic Rashba Effect in an Inversion-Symmetric Oxide, *Phys. Rev. Lett.* **108**, 206601 (2012).

Supplemental Material: Probing Fermi-surface spin-textures via the nonlinear Shubnikov-de Haas effect

PRELIMINARY REMARKS

The Hamiltonian of an electron system in an electromagnetic field is written as:

$$\hat{H}_0 = \frac{1}{2m}(\hat{\mathbf{p}} + e\mathbf{A})^2 = \frac{\hat{\mathbf{\Pi}}^2}{2m}, \quad (\text{S1})$$

where $\hat{\mathbf{p}} \equiv -i\hbar\mathbf{\nabla}$ and \mathbf{A} is the U(1) gauge field (vector potential). We note the commutation relation $[\hat{\Pi}_x, \hat{\Pi}_y] = -i\frac{\hbar^2}{\ell_B^2}$ with the squared magnetic length $\ell_B^{-2} \equiv |eB_z|/\hbar$. Assuming a static magnetic field and defining $\hat{a} = \frac{1}{\sqrt{2}}\frac{\ell_B}{\hbar}(\hat{\Pi}_x - i\hat{\Pi}_y)$ and $\hat{a}^\dagger = \frac{1}{\sqrt{2}}\frac{\ell_B}{\hbar}(\hat{\Pi}_x + i\hat{\Pi}_y)$ ($B_z > 0$ is assumed), we get

$$\hat{H}_0 = \hbar\omega_c \left(\hat{n} + \frac{1}{2} \right), \quad (\text{S2})$$

where $\hat{n} = \hat{a}^\dagger \hat{a}$ and the cyclotron frequency $\omega_c = \frac{|eB_z|}{m}$ with $\mathbf{B} = \mathbf{\nabla} \times \mathbf{A}$. Its eigenenergy take the form $\hbar\omega_c(n + 1/2)$ where n is an eigenvalue of \hat{n} . This is the simplest illustration of Landau-level formation. Each Landau level has macroscopic degeneracy, as one could define the operator $\hat{\mathbf{R}} = \hat{\mathbf{r}} + \frac{\ell_B^2}{\hbar}\hat{z} \times \hat{\mathbf{\Pi}}$ with $\hat{\mathbf{r}} = (\hat{x}, \hat{y})$, which commutes with the Hamiltonian. We denote this degeneracy per unit area as $N_L = (2\pi\ell_B^2)^{-1}$ in the main text. In this inversion-symmetric case, the second-order response vanishes.

FORMULATION OF THE NONLINEAR CONDUCTIVITY IN THE PRESENCE OF LANDAU LEVELS

The statistical average of the electric current can be calculated within the Keldysh formalism:

$$\langle \hat{j}_i \rangle = -\frac{i}{2} \int \frac{d\varepsilon}{2\pi} \text{tr}[\hat{j}_i \hat{G}^K(\varepsilon)]. \quad (\text{S3})$$

The Hamiltonian and the current operator are expanded in powers of $\mathbf{A}''(t)$ as

$$\hat{H}(\hat{\mathbf{\Pi}}) = \hat{H}(\hat{\mathbf{\pi}}) + \hat{\Gamma}_i A''_i(t) + \hat{\Gamma}_{ij} A''_i(t) A''_j(t) + \hat{\Gamma}_{ijl} A''_i(t) A''_j(t) A''_l(t) + \dots, \quad (\text{S4})$$

$$\hat{j}_i = \hat{\Lambda}_i + \hat{\Lambda}_{ij} A''_j(t) + \hat{\Lambda}_{ijl} A''_j(t) A''_l(t) + \dots, \quad (\text{S5})$$

where $\hat{\Gamma}_i, \hat{\Gamma}_{ij}, \hat{\Gamma}_{ijl}, \dots$ and $\hat{\Lambda}_i, \hat{\Lambda}_{ij}, \hat{\Lambda}_{ijl}, \dots$ are the expansion coefficients and the Einstein summation convention is employed for the spatial indices i, j, l . $\hat{G}^K(\varepsilon)$ can be expanded in terms of the coupling term $\hat{H}(\hat{\mathbf{\Pi}}) - \hat{H}(\hat{\mathbf{\pi}}) = \int \frac{d\omega}{2\pi} \hat{X}_i(-\omega) F_i(\omega)$ as

$$\hat{G}^K(\varepsilon) = \hat{G}^{K(0)}(\varepsilon) + \int \frac{d\omega}{2\pi} \hat{G}^{K(1)}(\varepsilon; \omega) + \iint \frac{d\omega}{2\pi} \frac{d\omega'}{2\pi} \hat{G}^{K(2)}(\varepsilon; \omega, \omega'), \quad (\text{S6})$$

$$\hat{G}^{K(0)}(\varepsilon) = (1 - 2f(\varepsilon))(\hat{G}^R(\varepsilon) - \hat{G}^A(\varepsilon)), \quad (\text{S7})$$

$$\hat{G}^{K(1)}(\varepsilon; \omega) = -2 \left[(f_+ - f_-) \hat{G}_+^R \hat{X}_i(-\omega) \hat{G}_-^A + f_- \hat{G}_+^R \hat{X}_i(-\omega) \hat{G}_-^R - f_+ \hat{G}_+^A \hat{X}_i(-\omega) \hat{G}_-^A \right] F_i(\omega), \quad (\text{S8})$$

$$\begin{aligned} \hat{G}^{K(2)}(\varepsilon; \omega, \omega') = & - \left[(f_{++} - f_{-+}) \hat{G}_{++}^R \hat{X}_i(-\omega) \hat{G}_{-+}^A \hat{X}_j(-\omega') \hat{G}_{--}^A + (f_{-+} - f_{--}) \hat{G}_{++}^R \hat{X}_i(-\omega) \hat{G}_{-+}^R \hat{X}_j(-\omega') \hat{G}_{--}^R \right. \\ & \left. + f_{++} \left\{ \hat{G}_{++}^A \hat{X}_i(-\omega) \hat{G}_{-+}^A \hat{X}_j(-\omega') \hat{G}_{--}^A \right\} - f_{--} \left\{ \hat{G}_{++}^R \hat{X}_i(-\omega) \hat{G}_{-+}^R \hat{X}_j(-\omega') \hat{G}_{--}^R \right\} F_i(\omega) F_j(\omega') \right] \\ & + (i, \omega \leftrightarrow j, \omega'). \end{aligned} \quad (\text{S9})$$

Here we define $F_i(\omega) = A''_i(\omega)$ and $\hat{X}_i(-\omega) = \hat{\Gamma}_i(-\omega) + \int \frac{d\omega'}{2\pi} \hat{\Gamma}_{ij}(-\omega - \omega') A''_j(\omega') + \int \frac{d\omega'}{2\pi} \int \frac{d\omega''}{2\pi} \hat{\Gamma}_{ijl}(-\omega - \omega' - \omega'') A''_j(\omega') A''_l(\omega'') + \dots$, and employ the notations $\varepsilon_\pm = \varepsilon \pm \hbar\omega/2$, $\varepsilon_{\pm\pm} = \varepsilon \pm \hbar\omega/2 \pm \hbar\omega'/2$, $x_\pm \equiv x(\varepsilon_\pm)$, and

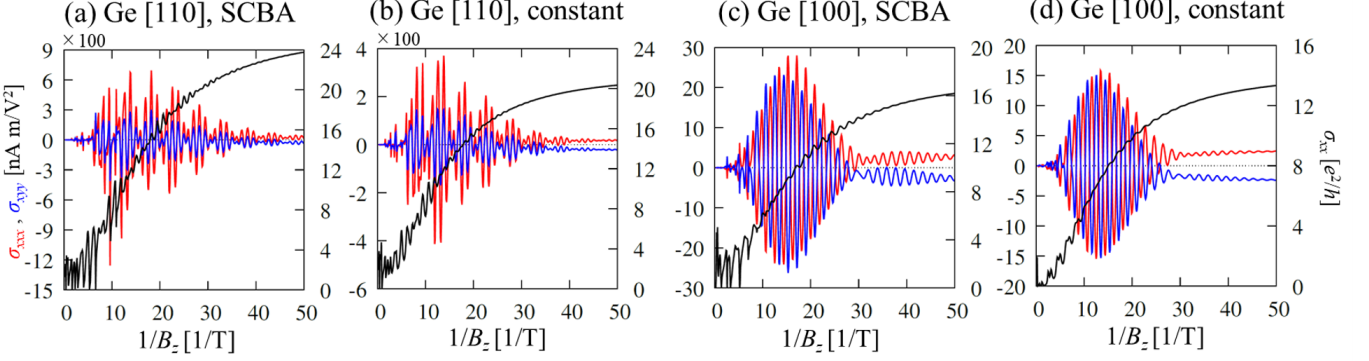


FIG. S1. The linear and nonlinear SdH oscillations in (a,b) Ge [110] parameters at $\mu = 1.5$ meV and (c,d) Ge [100] parameters at $\mu = 1$ meV in (a,c) self-consistent Born approximation (SCBA) with $n_i u^2 = 60$ meV² nm² and (b,d) imaginary constant self-energy of $i\gamma = 0.07i$ meV.

$x_{\pm\pm} \equiv x(\varepsilon_{\pm\pm})$. Keeping terms up to second order in the time-dependent vector potential $\mathbf{A}''(t)$ and taking the Fourier components at ω_1 and ω_2 , we obtain the second-order ac current $\langle \hat{j}_i^{(2)} \rangle(\omega_1, \omega_2)$ as

$$\begin{aligned} \langle \hat{j}_i^{(2)} \rangle(\omega_1, \omega_2) &= \frac{-i}{2\omega_1\omega_2} E_j(\omega_1) E_l(\omega_2) \int \frac{d\varepsilon}{2\pi} \\ &\times \text{tr} \left[f(\varepsilon) \left\{ 2\hat{\Gamma}_{ijl}(G^R - G^A) + \hat{\Lambda}_{ij}\hat{G}^R(\varepsilon + \hbar\omega_2)\hat{\Gamma}_l(G^R - G^A) + \hat{\Lambda}_{ij}(G^R - G^A)\hat{\Gamma}_l\hat{G}^A(\varepsilon - \hbar\omega_2) \right. \right. \\ &\quad + \hat{\Lambda}_{il}\hat{G}^R(\varepsilon + \hbar\omega_1)\hat{\Gamma}_j(G^R - G^A) + \hat{\Lambda}_{il}(G^R - G^A)\hat{\Gamma}_j\hat{G}^A(\varepsilon - \hbar\omega_1) \\ &\quad + 2\hat{\Lambda}_i\hat{G}^R(\varepsilon + \hbar\Omega)\hat{\Gamma}_{jl}(G^R - G^A) + 2\hat{\Lambda}_i(G^R - G^A)\hat{\Gamma}_{jl}\hat{G}^A(\varepsilon - \hbar\Omega) \\ &\quad + \hat{\Lambda}_i\hat{G}^R(\varepsilon + \hbar\Omega)\hat{\Gamma}_j\hat{G}^R(\varepsilon + \hbar\omega_2)\hat{\Gamma}_l(G^R - G^A) + \hat{\Lambda}_i\hat{G}^R(\varepsilon + \hbar\Omega)\hat{\Gamma}_l\hat{G}^R(\varepsilon + \hbar\omega_1)\hat{\Gamma}_j(G^R - G^A) \\ &\quad + \hat{\Lambda}_i\hat{G}^R(\varepsilon + \hbar\omega_1)\hat{\Gamma}_j(G^R - G^A)\hat{\Gamma}_l\hat{G}^A(\varepsilon - \hbar\omega_2) + \hat{\Lambda}_i\hat{G}^R(\varepsilon + \hbar\omega_2)\hat{\Gamma}_l(G^R - G^A)\hat{\Gamma}_j\hat{G}^A(\varepsilon - \hbar\omega_1) \\ &\quad \left. \left. + \hat{\Lambda}_i(G^R - G^A)\hat{\Gamma}_j\hat{G}^A(\varepsilon - \hbar\omega_1)\hat{\Gamma}_l\hat{G}^A(\varepsilon - \hbar\Omega) + \hat{\Lambda}_i(G^R - G^A)\hat{\Gamma}_l\hat{G}^A(\varepsilon + \hbar\omega_1)\hat{\Gamma}_j\hat{G}^A(\varepsilon - \hbar\Omega) \right\} \right] \\ &\equiv \sigma_{ijl}(\omega_1, \omega_2) E_j(\omega_1) E_l(\omega_2), \end{aligned} \quad (\text{S10})$$

where $\Omega = \omega_1 + \omega_2$ and we omit the ε dependence in $(G^R - G^A)$ for simplicity. When we take the dc limit, some $1/\omega$ -type terms appear; however, these terms can be disregarded because of causality (analytic continuation) [78]. Hence, the expression in the dc limit is

$$\langle \hat{j}_i^{(2)} \rangle = \sigma_{ijl} E_j E_l = (\sigma_{ijl}^{\text{DF}} + \sigma_{ijl}^{\text{F}}) E_j E_l, \quad (\text{S11})$$

$$\sigma_{ijl}^{\text{DF}} = \hbar^2 \int \frac{d\varepsilon}{2\pi} \left(-\frac{\partial f}{\partial \varepsilon} \right) \text{Im} \left[\text{tr} \left\{ \hat{\Lambda}_i \frac{\partial \hat{G}^R}{\partial \varepsilon} \left(\hat{\Gamma}_j \hat{G}^R \hat{\Gamma}_l + \hat{\Gamma}_{jl} \right) (\hat{G}^R - \hat{G}^A) \right\} \right] + (j \leftrightarrow l), \quad (\text{S12})$$

$$\sigma_{ijl}^{\text{F}} = -\hbar^2 \int \frac{d\varepsilon}{2\pi} f(\varepsilon) \text{Im} \left[\text{tr} \left\{ \hat{\Lambda}_i \frac{\partial \hat{G}^R}{\partial \varepsilon} \left(\hat{\Gamma}_j \hat{G}^R \hat{\Gamma}_l + \hat{\Gamma}_{jl} \right) \frac{\partial \hat{G}^R}{\partial \varepsilon} \right\} \right] + (j \leftrightarrow l). \quad (\text{S13})$$

This is very similar to previously derived formulas written in the wavenumber representation [55, 62, 74]. In addition, we can neglect the Fermi sea term σ_{ijl}^{F} since it is proportional to the damping factor and thus negligible in the clean and dc limit [62, 74]. Thus, we can straightforwardly obtain the diagonalized form noted in the main text.

ON THE COMPARISON BETWEEN SCBA AND IMAGINARY CONSTANT SELF ENERGY

Figure S1 shows the oscillations in σ_{xx} and σ_{xii} , comparing calculations performed using the self-consistent Born approximation and imaginary constant self-energy. Both approaches exhibit essentially the same features, and no qualitative differences are observed.

NONLINEAR CONDUCTIVITY UNDER THE IN-PLANE MAGNETIC FIELD

Here, we reexamine the calculation of the second-order nonlinear conductivity in the presence of an in-plane magnetic field [52–55] to discuss the relation between the spin texture on the band structure and the nonlinear response. We start from the $T = 0$ expression:

$$\sigma_{xii} \simeq -\frac{e^3}{\pi\hbar V} \text{Im} \sum_{\mathbf{k}} \text{tr} \left\{ \mathcal{V}_x (\mathcal{G}^R)^2 \left(\mathcal{V}_i \mathcal{G}^R \mathcal{V}_i + \frac{1}{2} \mathcal{V}_{ii} \right) \mathcal{G}^A \right\}, \quad (\text{S14})$$

where $\mathcal{G}^R \equiv (\mu - H_{\mathbf{k}} + i\gamma)^{-1} = (\mathcal{G}^A)^\dagger$ is retarded Green function with a constant purely imaginary self-energy $\hat{\Sigma}^R = -i\hbar/(2\tau) = -i\gamma$, $\mathcal{V}_i \equiv \partial_i H_{\mathbf{k}}$, and $\mathcal{V}_{ij} \equiv \partial_j \mathcal{V}_i$ [55, 62, 74]. The trace runs over the spin space. To clarify the dependence on the spin texture, we split the Hamiltonian into two parts as $H_{\mathbf{k}} = h_{\mathbf{k}} + \bar{\mathbf{S}}_{\mathbf{k}} \cdot \boldsymbol{\sigma}$ and assume a large μ and/or $h_{\mathbf{k}}$ for the perturbative treatment with respect to $\bar{\mathbf{S}}_{\mathbf{k}} \cdot \boldsymbol{\sigma}$. We also assume that $\mathbf{S}_{\mathbf{k}}$ should be an odd function of k_i . The perturbative expansion of the retarded/advanced Green function is expressed as

$$\mathcal{G}^{R(A)} = G^{R(A)} + G^{R(A)}(\bar{\mathbf{S}}_{\mathbf{k}} \cdot \boldsymbol{\sigma})G^{R(A)} + G^{R(A)}(\bar{\mathbf{S}}_{\mathbf{k}} \cdot \boldsymbol{\sigma})G^{R(A)}(\bar{\mathbf{S}}_{\mathbf{k}} \cdot \boldsymbol{\sigma})G^{R(A)} + \dots, \quad (\text{S15})$$

where $G^{R(A)} \equiv [\mu - h_{\mathbf{k}} \pm i\gamma]^{-1}$. The first-order perturbation vanishes because of $\text{tr } \sigma_i = 0$. The second-order contribution is crucial in our case. After straightforward calculations, we find

$$\begin{aligned} \sigma_{ijk} = & \frac{e^3}{\pi\hbar V} \text{Im} \sum_{\mathbf{k}} \left[(\partial_j \partial_k h_{\mathbf{k}})(\partial_i \bar{\mathbf{S}}_{\mathbf{k}}) \cdot \bar{\mathbf{S}}_{\mathbf{k}} + (\partial_k h_{\mathbf{k}})(\partial_j \partial_i \bar{\mathbf{S}}_{\mathbf{k}}) \cdot \bar{\mathbf{S}}_{\mathbf{k}} + (j \leftrightarrow k) \right] (G^R)^3 G^A \\ & + (i \rightarrow j \rightarrow k \rightarrow i) + (i \rightarrow k \rightarrow j \rightarrow i). \end{aligned} \quad (\text{S16})$$

The second term in Eq (S16) represents the curvature of the spin texture, which is relevant when the SOI term contains more than second-order of \mathbf{k} . This expression connects the geometry of spin texture on the band structure and the second-order nonlinear conductivity.

ON $\sigma_{xxx} = -\sigma_{xyy}$ FOR $\alpha = \beta_2 = 0$ CASE.

In the main text, we show that the phases of the oscillations in σ_{xxx} and σ_{xyy} are mutually opposite in the case of $\alpha = \beta_2 = 0$ and $\beta_1 \neq 0$, because of the relation

$$\sigma_{xxx} = -\sigma_{xyy}. \quad (\text{S17})$$

Here, we verify this relation by considering the symmetry of the model without the Zeeman interaction:

$$H_{\mathbf{k}} = \frac{\hbar^2 k^2}{2m^*} + i\beta_1(k_-^3 \sigma_+ - k_+^3 \sigma_-) \equiv \varepsilon_{0,\mathbf{k}} I + H_{\beta_1,\mathbf{k}}. \quad (\text{S18})$$

This model is invariant under the symmetry operations belonging to the point group C_{3v} . Let us set one of the mirror planes perpendicular to the y axis (the xz plane) which acts on polar and axial vectors (x, y, z) and (B_x, B_y, B_z) as $(x, -y, z)$ and $(-B_x, B_y, -B_z)$, respectively. The representation content and symmetry-adapted basis functions (up to the indicated orders) are summarized as follows.

C_{3v}	id	$2C_3$	$3\sigma_v$	Linear	Quadratic	$[\text{Quadratic, polar}] \times [\text{Higher order, axial}]$
A_1	1	1	1		$xx + yy$	$B_z^r (xx + yy)$ (with even r)
A_2	1	1	-1	B_z		$B_z^r (xx + yy)$ (with odd r)
\mathcal{E}	2	-1	0	$(x, y), (B_x, B_y)$	$(\mathcal{Q}_1 \text{Im} \mathcal{B}^n - \mathcal{Q}_2 \text{Re} \mathcal{B}^n, -\mathcal{Q}_1 \text{Re} \mathcal{B}^n - \mathcal{Q}_2 \text{Im} \mathcal{B}^n) B_z^m,$ $[(xx + yy) \text{Im} \mathcal{B}^n, -(xx + yy) \text{Re} \mathcal{B}^n] B_z^m$	

where A_1 , A_2 , and \mathcal{E} are the irreducible representations (irreps) and id , C_3 , and σ_v are the symmetry operations which stand for identity, three-fold rotation, and mirror operations, respectively, $n, m > 0$ are positive odd and even integer, $(\mathcal{Q}_1, \mathcal{Q}_2) = (x^2 - y^2, 2xy)$, and $\mathcal{B} \equiv B_x + iB_y$. We now restrict the discussion to the $\mathbf{B} = (0, B_y, B_z)$ case, on

which we focused in the main text. We find that the basis function $(\mathcal{Q}_1, -\mathcal{Q}_2)B_y^n B_z^m$ leads to a possible form of the current

$$j_x = (E_x^2 - E_y^2) \sum_{n,m} c_{nm} B_y^n B_z^m, \quad (\text{S19})$$

where c_{nm} is a coefficient. Eq. (S19) directly shows the “antisymmetric” relation $\sigma_{xxx} = -\sigma_{xyy}$. Similarly, we can show $\sigma_{yyy} = -\sigma_{yxx}$ by taking $\mathbf{B} = (B_x, 0, B_z)$.

Meanwhile, we also get undesired “symmetric” component from the basis function $(xx + yy)B_y^n B_z^m$:

$$j_x^{\text{sym}} = (E_x^2 + E_y^2) \sum_{n,m} c_{nm}^{\text{sym}} B_y^n B_z^m, \quad (\text{S20})$$

which hinder the exact relation $\sigma_{xxx} = -\sigma_{xyy}$. However, we can disregard this channel by considering the harmonicity of the cubic Rashba term, which is proven below.

Proof. Equation (S18) can be represented as

$$H_{\beta_1, \mathbf{k}} \equiv \beta_1(Q_{1,\mathbf{k}} \sigma_y - Q_{2,\mathbf{k}} \sigma_x), \quad (Q_{1,\mathbf{k}}, Q_{2,\mathbf{k}}) = (\text{Re}(k_x + ik_y)^3, \text{Im}(k_x + ik_y)^3).$$

Hereafter, we focus on the $H_{\beta_1, \mathbf{k}}$ term since any nonequilibrium (transport) current arising from $\varepsilon_{0,\mathbf{k}}$ vanishes due to inversion symmetry. The in-plane electric field, in-plane magnetic field, and out-of-plane magnetic field transforms as the polar \mathcal{E}_p , the axial \mathcal{E}_a and the scalar A_2 irreps, respectively. The output current transforms as \mathcal{E}_p . We need a symmetric square

$$\text{Sym}^2 \mathcal{E}_p = A_1 \oplus \mathcal{E}_p.$$

to consider the second-order input. Let us introduce the linear map

$$\tilde{\sigma}^{(2)} : \text{Sym}^2 \mathcal{E}_p \otimes \text{Sym}^n \mathcal{E}_a \otimes (A_2)^{\otimes m} \otimes \mathcal{F} \rightarrow \mathcal{E}_p. \quad (\text{S21})$$

Here \mathcal{F} , the scalar coefficients, collects all material-dependent ingredients (integrations and/or summations of the products of Green functions, distribution function, etc.). Let $P_{A_1}, P_{\mathcal{E}_p} : \text{Sym}^2 \mathcal{E}_p \rightarrow \text{Sym}^2 \mathcal{E}_p$ be the projectors onto A_1 and \mathcal{E}_p , respectively. For any $\tilde{\sigma}^{(2)}$,

$$\tilde{\sigma}^{(2)} = \tilde{\sigma}^{(2)} \circ (P_{A_1} \otimes \text{id} \otimes \text{id} \otimes \text{id}) + \tilde{\sigma}^{(2)} \circ (P_{\mathcal{E}_p} \otimes \text{id} \otimes \text{id} \otimes \text{id}) = \tilde{\sigma}_{A_1}^{(2)} + \tilde{\sigma}_{\mathcal{E}_p}^{(2)},$$

which correspond to the A_1 (symmetric) and \mathcal{E}_p (antisymmetric) components of the nonlinear conductivity, respectively. Then, consider the symmetric Hessian $\mathcal{D}_{jl}(F) \equiv \partial_{k_j} \partial_{k_l} F$ as an element of $\text{Sym}^2 \mathcal{E}_p$. In case of two-dimensional systems, the A_1 -projection is the trace (Laplacian):

$$P_{A_1} [\mathcal{D}_{jl}(F)] = \frac{1}{2} (\partial_{k_x}^2 + \partial_{k_y}^2) F \delta_{jl} = \frac{1}{2} \Delta_{\mathbf{k}} F \delta_{jl}. \quad (\text{S22})$$

The cubic polynomials $Q_{1,\mathbf{k}}, Q_{2,\mathbf{k}}$ are two-dimensional harmonics, hence $\Delta_{\mathbf{k}} H_{\beta_1, \mathbf{k}} = 0$. Plugging $F = H_{\beta_1, \mathbf{k}}$ gives

$$P_{A_1} [\mathcal{D}_{jl}(H_{\beta_1, \mathbf{k}})] = \frac{1}{2} \Delta_{\mathbf{k}} H_{\beta_1, \mathbf{k}} \delta_{jl} = 0.$$

Therefore, in the present model, the A_1 -channel coefficient is fixed to zero by β_1 -harmonicity: $\tilde{\sigma}_{A_1}^{(2)} = 0$. \square

Therefore, only the component that satisfies $\sigma_{xxx} = -\sigma_{xyy}$ or $\sigma_{yyy} = -\sigma_{yxx}$ can remain finite in the Hamiltonian Eq. (S18).

NONLINEAR RESISTIVITY

The primary experimental observable is the resistivity, rather than the conductivity. We therefore provide the nonlinear resistivity ρ_{xii} , which is generally a linear combination of nonlinear conductivities, assuming the model we discussed in the main text [54]:

$$\rho_{xxx} = -\rho_{xx}^3 \sigma_{xxx} - \rho_{xx} \rho_{xy}^2 \sigma_{xyy}, \quad (\text{S23})$$

$$\rho_{xyy} = -\rho_{xx}^3 \sigma_{xyy} - \rho_{xx} \rho_{xy}^2 \sigma_{xxx}, \quad (\text{S24})$$

where ρ_{ij} is the linear resistivity tensor. We now focus on the weak magnetic field regime and make reasonable simplifying assumptions for the linear resistivity. First, we assume that the Hall resistivity is given by $\rho_{xy} = AB_z \rho_{xx}$, where $A \sim 10 \text{ T}^{-1}$ [48]. Second, we neglect the oscillatory component of ρ_{xx} and take the zero field value $\rho_{xx} \sim \rho_0$, while retaining the oscillating component $\sigma_{xii} \sim \sigma_{xii}^{\text{osc}}$ deduced from our observations in the main text. Substituting these approximations into Eqs. (S23) and (S24), we get

$$\frac{\rho_{xxx}}{\rho_0} = -\rho_0^2 [\sigma_{xxx}^{\text{osc}} - (AB_z)^2 \sigma_{xyy}^{\text{osc}}], \quad (\text{S25})$$

$$\frac{\rho_{xyy}}{\rho_0} = -\rho_0^2 [\sigma_{xyy}^{\text{osc}} - (AB_z)^2 \sigma_{xxx}^{\text{osc}}]. \quad (\text{S26})$$

Under the weak field regime ($AB_z < 1$, $B_z < 0.1 \text{ T}$), we arrive at

$$\rho_{xxx} \simeq -\rho_0^3 \sigma_{xxx}^{\text{osc}}, \quad (\text{S27})$$

$$\rho_{xyy} \simeq -\rho_0^3 \sigma_{xyy}^{\text{osc}}, \quad (\text{S28})$$

which means that the ρ_{xii} is governed by a single component of the nonlinear conductivity. Moreover, in the β_1 -only model, Eqs. (S23) and (S24) satisfy the relation

$$\rho_{xxx} = -\rho_{xyy}, \quad (\text{S29})$$

because $\sigma_{xxx} = -\sigma_{xyy}$ is satisfied in this model, as shown in Sec. . To conclude, we can observe the same features as in the nonlinear conductivities in the nonlinear resistivities.